Sādhanā (2021)46:98
https://doi.org/10.1007/s12046-021-01588-2

Existence of boundary layer nanofluid flow through a divergent channel in porous medium with mass suction/injection

AJEET KUMAR VERMA[1], ANIL KUMAR GAUTAM[1], KRISHNENDU BHATTACHARYYA[1,*] and R P SHARMA[2]

[1]Department of Mathematics, Institute of Science, Banaras Hindu University, Varanasi 221005, India
[2]Department of Basic and Applied Science, National Institute of Technology, Yupia 791112, India
e-mail: krishmath@bhu.ac.in

MS received 23 May 2020; revised 7 January 2021; accepted 13 January 2021

Abstract. The steady two-dimensional, laminar, viscous, incompressible boundary layer flow of Cu/Ag-H_2O nanofluid in a diverging channel formed by two non-parallel walls in a Darcian porous medium is numerically studied in the presence of mass suction/injection of equal magnitude on both the walls. Here, divergent flow is generated by a line source of fluid volume at the intersection of channel walls. Using similarity transformations, the non-linear governing PDEs are transformed into self-similar coupled non-linear ODEs and they are solved numerically with the help of MATLAB-built solver "bvp4c". The conditions for the existence of boundary layer flow structure for nanofluid through divergent channel in porous medium are obtained. The analysis reveals that when the permeability parameter K and nanofluid-volume-fraction-related parameter ϕ_1 are chosen in a specific manner such that they satisfy the condition $K > 2\phi_1$ then boundary layer flow exists, preventing separation for any mass suction/injection or even in the absence of mass suction/injection. A similar velocity field rises with permeability parameter, which exhibits opposite behavior with nanoparticle volume fraction. Also temperature increases with nanoparticle volume fraction, permeability parameter, and Eckert number, and decreases with power-law exponent (related to variable wall temperature). Skin-friction coefficient and heat transfer rate for Cu-water nanofluid are stronger when compared with Ag-water nanofluid.

Keywords. Existence of boundary layer; Nanofluid; Divergent channel; Porous medium; Mass suction/injection.

1. Introduction

The enhancement in heat transfer of regular fluids (water, ethylene glycol, engine oil, etc.) can be done by altering flow situation, (like convective boundary condition, partial slip, etc.), different flow parameters, or by augmenting thermal conductivity of the fluid. Many theoretical techniques have been introduced to enhance heat transfer in regular fluids. Thus researchers believe that nano- or larger sized colloidal suspensions of particles can enhance the thermal conductivity of carrier fluids, but because of deficiency in the stability of the larger sized (micro/milli meter sized) colloidal composition and its larger resistance to the flow (as confirmed by many experimental and theoretical studies) this treatment is not able to gain popularity. Later the research communities use the idea that thermal conductivities of classical fluids can be augmented by a colloidal suspension of nanometer-sized particles of metals, oxides, carbides, nitrides, etc., and they find that they are more efficient and useful than micro-sized particles. The term nanofluid was established firstly by Choi [1]. It has a wide range of practical applications in many fields of science and engineering, namely petroleum reservoirs, geothermal systems, heat exchangers, etc., because of its higher thermal conductivity and heat transfer capacity. Later, Sheikholeslami *et al* [2] analyzed the influence of magnetic field and nanoparticle on flow in convergent/divergent channels. Usman *et al* [3] studied heat transfer of water-based fluid with metallic nanoparticles along the converging/diverging channel and solved the problem using the well-known least-square method. They considered two types of nanoparticles: Cu and Ag, and detailed comparative analyses were reported. The nanofluid flow between two inclined planes under the influence of magnetic field was done by Biswal and Charkraverty [4]. Azimi and Riazi [5] studied analytically the flow of MHD Cu-water nanofluid through convergent/divergent channels. Recently, nanofluid flow and heat transfer through porous media attracted substantial attention of researchers because of their important properties regarding heat transfer

*For correspondence
Published online: 06 May 2021

enhancement. It has abundant applications in environmental or industrial problems, such as thermal insulation, filtration process, storage of nuclear waste, drying process, fuel cells, and geothermal systems. Heat transfer analysis of nanofluid through diverging/converging channel in porous medium was done by Akinshilo *et al* [6], whereas free convective nanofluid flow in an inclined square in porous medium was discussed by Alsaberry *et al* [7].

Vagueness in existence of boundary layer structure in neighborhood of two-channel walls inclined at some fixed angle to the flow of an incompressible, viscous fluid through a divergent/convergent channel is one of the crucial problems in fluid dynamics. Such problems were first studied by Jeffery [8] and Hamel [9]. In this type of problems, flow occurs due to the presence of source/sinks of fluid volume at the intersection of two channel walls and it results in either a divergent or a convergent flow. An analytical solution of convergent flow for velocity field was obtained by Pohlhausen [10] and the temperature distribution was discussed by Millsaps and Pohlhausen [11]. The renowned researchers Harison [12], Tollmien [13], Noether [14], and Dean [15] discussed some remarkable characteristics of this flow. Later, MHD boundary layer of power-law non-Newtonian fluid in a diverging permeable channel with suction/injection was analyzed by Bhattacharyya and Layek [16]. Dogonchi and Ganji [17] discussed MHD flow of water-based nanofluid in a stretchable/shrinkable convergent/divergent channel with effects of thermal radiation. Mohyud-Din *et al* [18] described Buongiorno's model nanofluid in a MHD stretchable convergent/divergent channel flow with heat and mass transfer and solved using the RKF (Runge–Kutta–Fehlberg) method. Rana *et al* [19] obtained dual analytical solutions (HAM solutions) of Jeffery–Hamel MHD flow with Koo–Kleinstreuer–Li (KKL) alumina model and numerical solutions by RKF confirmed the accuracy of analytical solutions. Kumar *et al* [20] analyzed the improvement of thermal properties in a convergent/divergent channel flow in non-Darcy porous medium due to the presence of carbon nanotubes and pointed out a vital remark that the heat transfer is stronger for the divergent flow compared with that of the convergent flow.

Similarity solutions for these problems, in which flow is purely radial and contains only one velocity component, are obtained in polar co-ordinates. It prevails that for any finite Reynolds number and any channel angle, a convergent symmetrical flow exists and two identical irrotational boundary layer flows occur on the channel walls. On the contrary a purely divergent flow exists for a given channel angle, and for Reynolds number less than a critical value. If Reynolds number exceeds the critical value, then the divergent flow near one of the channel walls has a region of inflow (i.e., backflow). In the solutions, many more regions of inflow and outflow are witnessed as Reynolds number augments further and those regions enlarge. The viscosity effect is dominant everywhere in the flow and width of each region of outflow becomes small. Thus, boundary layer solution without separation becomes impossible in the diverging channel compared with the convergent channel at large Reynolds number. For very small magnetic Reynolds number both convergent and divergent flows were analyzed by Jungclaus [21] and for large Reynolds number the MHD divergent flow was studied by Layek *et al* [22]. Later on, some more key characteristics of divergent/convergent channel flow were discussed in literature by some researchers [23–25].

Aforesaid separation phenomenon in the form of backflow and its prevention in diverging channel flow of nanofluid motivate us towards this venture. Hence, the steady, incompressible, laminar, viscous, divergent channel flow of Cu/Ag-H_2O nanofluid in porous medium with suction/injection is studied. A self-similar boundary layer solution for this problem exists only with suitable presence of mass suction/injection. The intention of this investigation is to explore the effects of porous medium resistance and nanoparticles volume fraction on the existence conditions of boundary layer in divergent channels and when boundary layer flow exists how it affects the velocity distribution and temperature field for two types of nanofluids, namely Cu-H_2O and Ag-H_2O nanofluids. The novelty of the present study lies in the fact that when permeability parameter and nanoparticle-volume-fraction-related parameter are specified suitably (as discussed in section 3), the boundary layer solutions (without separation) exist for the diverging channel without any condition on suction and even in the presence of injection at the porous walls.

2. Mathematical formulation

Consider the steady, laminar, two-dimensional, boundary layer flow of an incompressible nanofluid through a divergent channel in a porous medium. The walls of divergent channel are assumed to be stationary and permeable, which are subjected to suction/injection. It is expected that the flow (when it exists) will be symmetrical about the central line of the channel. A physical sketch of the problem is given in figure 1. The steady boundary layer equations in Darcy porous medium may be written as [22, 26, 27] follows:

$$\frac{\partial u}{\partial x}+\frac{\partial v}{\partial y}=0 \tag{1}$$

$$u\frac{\partial u}{\partial x}+v\frac{\partial u}{\partial y}=-\frac{1}{\rho_{nf}}\frac{\partial p}{\partial x}+\upsilon_{nf}\frac{\partial^2 u}{\partial y^2}-\frac{\upsilon_{nf}}{k}u \tag{2}$$

$$0 = -\frac{1}{\rho_{nf}}\frac{\partial p}{\partial y} \tag{3}$$

$$u\frac{\partial T}{\partial x} + v\frac{\partial T}{\partial y} = \frac{\kappa_{nf}}{(\rho c_p)_{nf}}\frac{\partial^2 T}{\partial y^2} + \frac{\mu_{nf}}{(\rho c_p)_{nf}k}u^2 \tag{4}$$

where u and v are the velocity components in x- and y-directions, respectively, p is the pressure, υ_{nf} is the nanofluid kinematic viscosity, k $(= k_0 x^2)$ is the variable permeability of porous medium, T is the temperature of nanofluid, $(\rho c_p)_{nf}$ is the heat capacity of nanofluid, κ_{nf} is the nanofluid thermal conductivity, μ_{nf} is the viscosity of nanofluid fluid, and ρ_{nf} is the density of nanofluid, which are given as follows [28]:

$$\left.\begin{aligned} &\rho_{nf} = (1-\phi)\rho_f + \phi\rho_s,\ \mu_{nf} = \frac{\mu_f}{(1-\phi)^{2.5}},\ \upsilon_{nf} = \frac{\mu_{nf}}{\rho_{nf}},\\ &(\rho c_p)_{nf} = (1-\phi)(\rho c_p)_f + \phi(\rho c_p)_s,\ \frac{\kappa_{nf}}{\kappa_f} = \frac{(\kappa_s + 2\kappa_f) - 2\phi(\kappa_f - \kappa_s)}{(\kappa_s + 2\kappa_f) + \phi(\kappa_f - \kappa_s)}. \end{aligned}\right\} \tag{5}$$

Here, ϕ is the nanoparticle volume fraction; ρ_f and ρ_s are densities of fluid and solid fractions, respectively; κ_f and κ_s are fluid and solid fraction thermal conductivities, respectively. The expression for κ_{nf}/κ_f used here is restricted to spherical nanoparticles only. Here two types of nanoparticles, namely copper and silver, and water as base fluid are considered and their thermal properties are given in table 1. On estimating orders of two momentum equations, it follows that $|\partial p/\partial y| << |\partial p/\partial x|$. This means that in boundary layer flow, p is, to a first approximation, a function of x only, which justifies Eq. (3).

The boundary conditions are

$$u = 0,\ v = -v_w(x) \text{ at } y = 0,\ u \to U(x) \text{ for } x > 0 \text{ as } y \to \infty, \tag{6}$$

$$T = T_w = T_\infty + T_0 x^n \text{ at } y = 0;\ T \to T_\infty \text{ as } y \to \infty \tag{7}$$

No-slip boundary conditions are considered and the variable free-stream velocity U is given by [22, 29]:

$$U(x) = \frac{Q}{\alpha x} = \frac{U_0 L}{x}\ (U_0 > 0) \tag{8}$$

where α is the angle of the channel assumed to be small, Q (>0) is a constant, U_0 is the characteristic velocity, and L is the characteristic length along the direction of the motion (with $Q/\alpha = U_0 L$).

The applied mass suction/injection velocity $v_w(x)$ through porous channel wall is given by

$$v_w(x) = \frac{S\sqrt{Q\upsilon_f}}{x\sqrt{\alpha}} \tag{9}$$

where S is the mass suction/injection parameter ($S > 0$ for suction and $S < 0$ for injection). This type of consideration of the mass suction/injection velocity is in view of the similarity solution for the velocity field (see Layek *et al* [22]). Here T_w is the variable temperature along channel walls, T_0 is a constant that depends on thermal properties of the fluid, T_∞ is the fixed temperature of free-stream flow, and n is the power-law exponent.

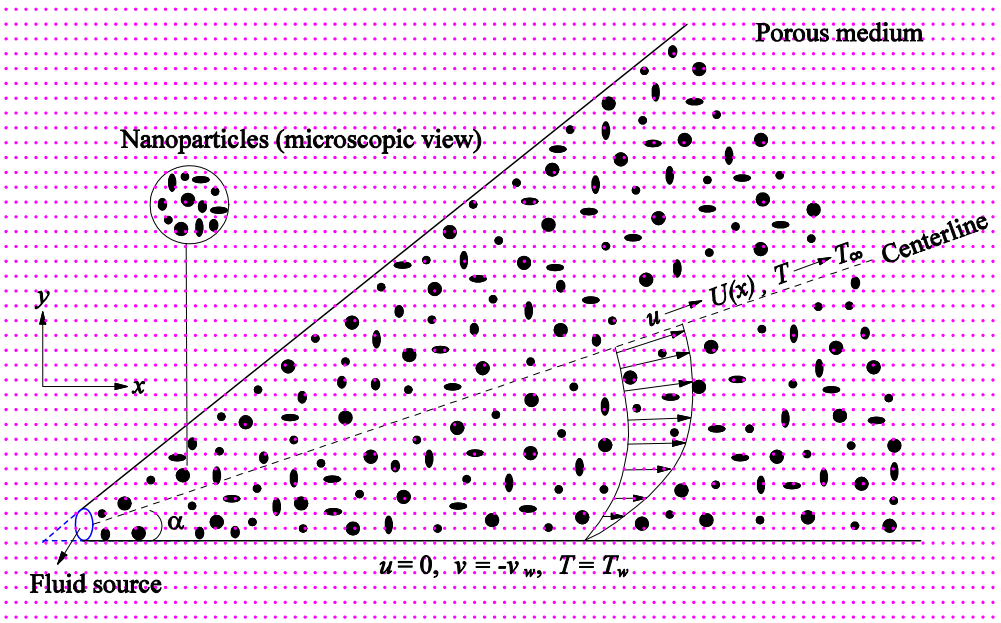

Figure 1. Physical sketch of the problem.

Table 1. Thermophysical properties of water, copper, and silver nanoparticles.

Physical properties	Water (H_2O)	Copper (Cu)	Silver (Ag)
C_p (J/kg K)	4179	385	235.0
ρ (kg/m^3)	997.1	8933	10500
κ (W/m K)	0.613	401	429

From (3), it is clear that the pressure p is a function of x only and also pressure gradient $\partial p/\partial x$ can now be obtained from (2) using the free-stream condition in (6) as

$$-\frac{1}{\rho_{nf}}\frac{\partial p}{\partial x} = U\frac{dU}{dx} + \frac{\upsilon_{nf}}{k}U \tag{10}$$

Eliminating $\partial p/\partial x$ from (2) using (10), we get

$$u\frac{\partial u}{\partial x} + v\frac{\partial u}{\partial y} = U\frac{dU}{dx} + \upsilon_{nf}\frac{\partial^2 u}{\partial y^2} + \frac{\upsilon_{nf}}{k}(U-u) \tag{11}$$

This system of equations admits the following similarity solution [22]:

$$\left.\begin{aligned} u = \frac{Q}{\alpha x}f(\eta) \text{ and } v = \sqrt{\frac{Q\upsilon_f}{\alpha}}[\eta f(\eta) - S] \\ T = T_\infty + (T_w - T_\infty)\theta(\eta) \end{aligned}\right\Big/ x \tag{12}$$

where $\eta = (y/x)\sqrt{Q/(\alpha\upsilon_f)}$ is the similarity variable.

On using Eq. (12) and the similarity variable, the equation of continuity (1) is satisfied automatically and Eqs. (11) and (4) take the following self-similar forms:

$$\frac{1}{\phi_1}f'' - (1-f^2) + \frac{K}{\phi_1}(1-f) + Sf' = 0 \tag{13}$$

$$\frac{1}{\phi_2}\frac{\kappa_{nf}}{\kappa_f}\theta'' + \Pr(S\theta' - nf\theta) + \frac{\phi_3}{\phi_2}\Pr KEcf^2 = 0 \tag{14}$$

where $K = \frac{\upsilon_f \alpha}{k_0 Q}$ is the permeability parameter, $\Pr = \frac{\upsilon_f(\rho c_p)_f}{\kappa_f}$ is the well-known Prandtl number, and $Ec = \frac{U^2}{(c_p)_f(T_w - T_\infty)}$ is the Eckert number; nanoparticle-volume-fraction-related parameters ϕ_1, ϕ_2, and ϕ_3 are given by $\phi_1 = (1-\phi)^{2.5}\left(1-\phi+\phi\frac{\rho_s}{\rho_f}\right)$, and $\phi_2 = (1-\phi)+\phi\frac{(\rho c_p)_s}{(\rho c_p)_f}$, $\phi_3 = \frac{1}{(1-\phi)^{2.5}}$ and the boundary conditions become

$$\left.\begin{aligned} f(0) = 0,\ f(\infty) = 1, \\ \theta(0) = 1,\ \theta(\infty) = 0. \end{aligned}\right\} \tag{15}$$

Physical quantities of practical interest, i.e. local skin-friction coefficient and local Nusselt number, are given as follows:

$$C_f = \frac{\tau_w}{\rho_f U^2} \text{ and } \mathrm{Nu}_x = \frac{xq_w}{\kappa_f(T_w - T_\infty)}, \tag{16}$$

$$\text{where } \tau_w = \mu_{nf}\left(\frac{\partial u}{\partial y}\right)_{y=0} \text{ and } q_w = -\kappa_{nf}\left(\frac{\partial T}{\partial y}\right)_{y=0}. \tag{17}$$

Using Eqs. (8), (12), and (17) in Eq. (16), we get

$$C_f \mathrm{Re}_x^{1/2} = \frac{1}{(1-\phi)^{2.5}}f'(0) \text{ and } Nu_x \mathrm{Re}_x^{-1/2} = -\frac{\kappa_{nf}}{\kappa_f}\theta'(0) \tag{18}$$

where $\mathrm{Re}_x = \frac{Ux}{\upsilon_f}$ is the local Reynolds number.

3. Existence of boundary layer and its conditions

Under certain restriction on flow parameters, flow separation can be controlled by preventing backflow; i.e., inflow and boundary layer structure for nanofluid flow through a divergent channel in a porous medium are possible. Inside the region of boundary layer flow, the quantity $f'(\eta)$ is proportional to velocity gradient $\partial u/\partial y$. Since across the boundary layer $\partial u/\partial y$ gradually decreases and tends to 0 at the edge of boundary layer, it follows that $Y[=f'(\eta)]$ is a decreasing function of η so that $Y'(\eta)<0$ inside boundary layer and $Y\to 0$ as $\eta\to\infty$. Now as η varies from 0 to ∞, $f(\eta)$ increases from 0 (its value at the wall) to 1 (its value at the edge of boundary layer) so that $f'(\eta)>0$. Hence, $\partial Y/\partial f = (\partial Y/\partial\eta)/(\partial f/\partial\eta)$ is negative inside boundary layer and $Y\to 0$ as $f\to 1$ [22].

Using $Y = f'(\eta)$ and $f''(\eta) = Y(\partial Y/\partial f)$, the self-similar equation (13) may be written as follows:

$$\frac{dY}{df} = \frac{\phi_1(1-f^2) - S\phi_1 Y - K(1-f)}{Y} \tag{19}$$

On taking the limit $f\to 1$, this equality (19) becomes

$$\lim_{f\to 1}\frac{dY}{df} = \lim_{f\to 1}\frac{\phi_1(1-f^2) - S\phi_1 Y - K(1-f)}{Y}$$

As right-hand side of the limit takes an indeterminate form, we have

$$\lim_{f\to 1}\frac{dY}{df} = \lim_{f\to 1}\frac{-2\phi_1 f - S\phi_1\frac{dY}{df} + K}{\frac{dY}{df}}$$

$$\Rightarrow \lim_{f\to 1}\frac{dY}{df} = \frac{-2\phi_1 - S\phi_1 \lim\limits_{f\to 1}\frac{dY}{df} + K}{\lim\limits_{f\to 1}\frac{dY}{df}}.$$

Denoting $(\partial Y/\partial f)_{f\to 1} = G$, we have

$$G^2 + S\phi_1 G + 2\phi_1 - K = 0 \tag{20}$$

which gives

$$G = \frac{1}{2}\left\{-S\phi_1 \pm \sqrt{S^2\phi_1^2 + 4(K - 2\phi_1)}\right\} \tag{21}$$

For the existence of boundary layer flow, the value of G should be negative across the boundary layer region. If the permeability parameter $K > 2\phi_1$, then one of the two values of G is negative for all possible values of S (i.e., it may be mass suction, $S>0$, or mass injection, $S < 0$, or without suction/injection, $S = 0$); hence boundary layer flow will exist near both channel walls. Hence, in the presence of a porous medium with suitable value of permeability parameter in diverging channel flow, nanofluid separation can be prevented and also it confirms existence of a self-similar boundary layer solution with a lower level of suction velocity and even for injection. This is the noteworthy result of the present analysis. The value of ϕ_1 (with any ϕ) for Ag-nanoparticles is larger than that for Cu-nanoparticles. Hence, the required value of K for existence of boundary layer with any value of S is larger for Ag-H_2O nanofluid than it is for Cu-H_2O nanofluid. Also, for $\phi_1 = 1$ ($\phi = 0$, no nanoparticle) and $K = 0$ (without porous medium), when suction parameter $S \geq 2\sqrt{2}$ then in the diverging channel, self-similar boundary layer flow (without separation) is possible, which is reported by Holstien [30]. These results are likely to have practical applications for flow in a diffuser. Another novel result of this analysis is that boundary layer nanofluid flow (without separation) in the diverging channel is possible even in the presence of injection at the walls. Next, if $K<2\phi_1$ and $S^2\phi_1^2<4(2\phi_1 - K)$ then values of G are imaginary so boundary layer flow is not possible and also if $K<2\phi_1$ and $S^2\phi_1^2 > 4(2\phi_1 - K)$ then both values of G are negative only when $S>0$ (i.e. mass suction) so boundary layer flow exists; however, when $S<0$ (i.e. mass injection) then both values of G should be positive; therefore, no boundary layer flow is possible in case of mass injection. Now, if $K = 2\phi_1$ and if $K<2\phi_1$ and $S^2\phi_1^2 = 4(2\phi_1 - K)$ then G has negative value only when $S>0$ and consequently boundary layer flow exists for suction only.

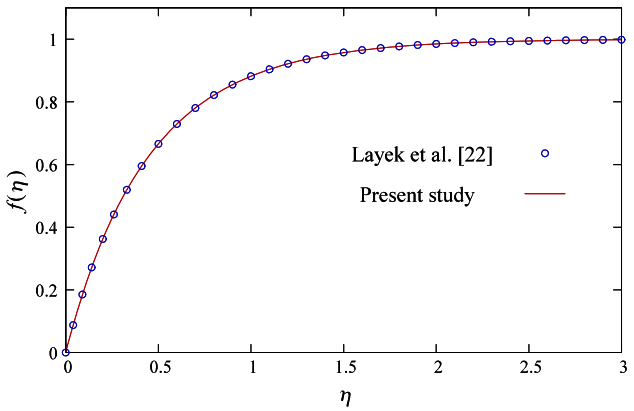

Figure 2. Comparison of velocity profile with that of Layek *et al* [22] for $\phi = 0$, $K = 0$, and $S = 3$.

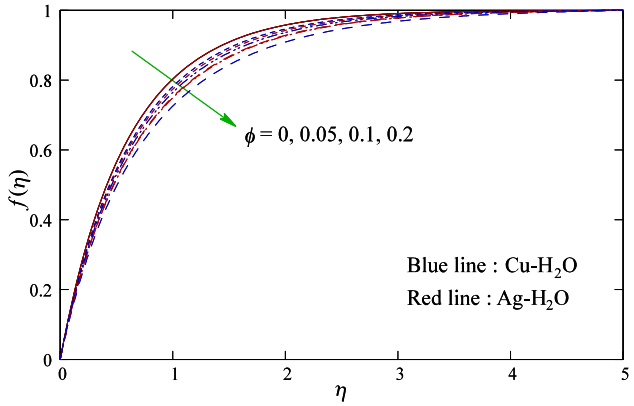

Figure 3. Velocity profile for various values of ϕ with $K = 4$, $S = 0.2$, $Ec = 0.03$, $n = 1$, and Pr = 6.2.

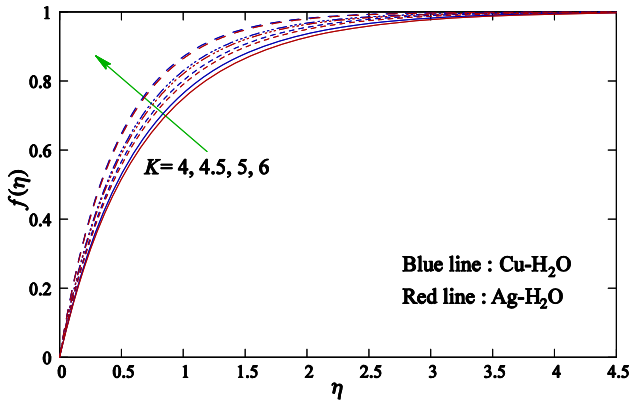

Figure 4. Velocity profile for various values of K with $\phi = 0.1$, $S = 0.2$, $Ec = 0.03$, $n = 1$, and Pr = 6.2.

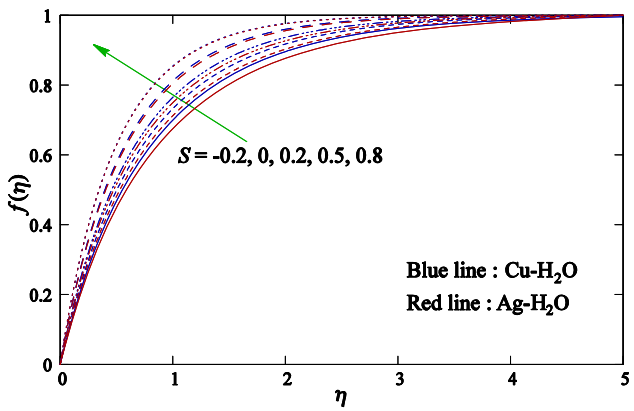

Figure 5. Velocity profile for various values of S(suction/injection) with $\phi = 0.1$, $K = 4$, $Ec = 0.03$, $n = 1$, and Pr = 6.2.

4. Numerical solution and discussion

The coupled nonlinear higher-order flow governing differential equations (13) and (14) with boundary conditions in (15) are solved numerically using the MATLAB-built package "bvp4c". To solve using "bvp4c" this problem is converted to an IVP with set of first-order ODEs and to do this, new variables are introduced as follows:

$$\left.\begin{aligned} y_1' = y_2,\ y_2' = \phi_1\left(1-y_1^2\right) - K(1-y_1) - S\phi_1 y_2, \\ y_3' = y_4,\ y_4' = \phi_2 \Pr\left(n y_1 y_3 - S y_4 - \frac{\phi_3 KEc}{\phi_2} y_1^2\right) \Big/ \frac{\kappa_{nf}}{\kappa_f}, \end{aligned}\right\} \tag{22}$$

with $f(\eta) = y_1(\eta)$ and $\theta(\eta) = y_3(\eta)$.

The bvp4c is a finite-difference code that executes the three-stage Lobatoo IIIa formula, which is a collocation formula, and the collocation polynomial provides a C^1-continuous solution and has fourth-order accuracy uniformly in the interval of integration. Error control in the solution is based on residual error; the tolerance level is set to the order of 10^{-5}. To get the almost continuous solutions, a suitable guess of initial conditions is selected and also they are chosen in a way such that the solutions show asymptotic convergence to the boundary conditions.

To affirm the accurateness of numerical scheme a comparison of velocity profile with that of Layek *et al* [22] is presented in figure 2 for pure water in the absence of porous medium and the results are in excellent agreement. Hence, one can confidently comment that the afore-mentioned numerical scheme produces correct results. After confirming the accuracy the numerical computation is carried out and the numerical solutions are plotted in some figures for all involved physical parameters, viz. nanoparticle volume fraction ϕ, permeability parameter K, suction/injection parameter S, Eckert number Ec, power-law exponent n, and Prandtl number parameter Pr. In numerical computations the constant values of parameters, when they are not varied, are taken as follows: $\phi = 0.1$, $K = 4$, $S = 0.2$, $n = 1$, $Ec = 0.03$, and $\Pr = 6.2$.

Figures 3–5 exhibit the exact effects of ϕ, K, and $S(>0$ and $<0)$ on velocity $f(\eta)$. From figure 3, it is pretty clear that velocity declines as ϕ increases and

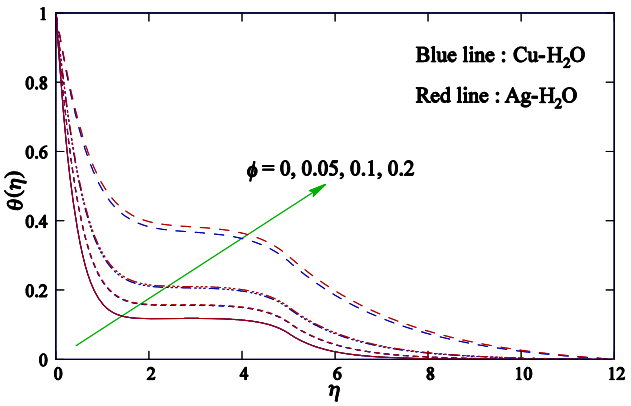

Figure 6. Temperature profile for various values of ϕ with $K = 4$, $S = 0.2$, $Ec = 0.03$, $n = 1$, and $\Pr = 6.2$.

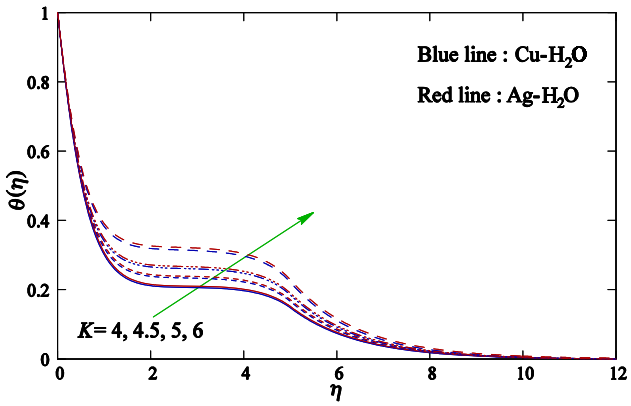

Figure 7. Temperature profile for various values of K with $\phi = 0.1$, $S = 0.2$, $Ec = 0.03$, $n = 1$, and $\Pr = 6.2$.

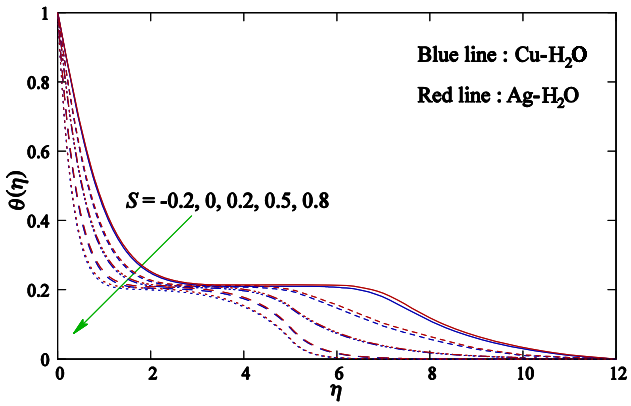

Figure 8. Temperature profile for various values of S(suction/injection) with $\phi = 0.1$, $K = 4$, $Ec = 0.03$, $n = 1$, and $\Pr = 6.2$.

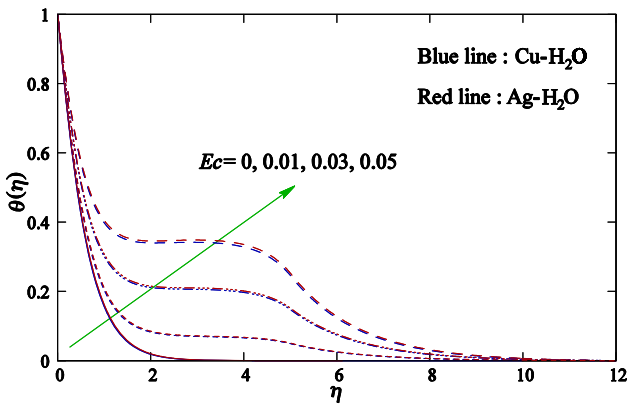

Figure 9. Temperature profile for various values of Ec with $\phi = 0.1$, $K = 4$, $S = 0.2$, $n = 1$, and $\Pr = 6.2$.

corresponding momentum boundary layer becomes thick for both Cu-H_2O and Ag-H_2O nanofluids. Also, from this figure, it is also noted that the decrement in velocity is larger in Ag-water nanofluid compared with Cu-water nanofluid. Figure 4 depicts that the velocity is augmented with permeability parameter K, though there is a reduction in boundary layer width, and in addition, increment in velocity for Cu-H_2O nanofluid is larger compared with Ag-H_2O nanofluid for smaller K values; as K grows the difference in velocity of Cu-H_2O and Ag-H_2O nanofluids diminishes. Physically, for larger K, friction and interactions between nanoparticles grow, which result in enhancement of velocity. Hence, it is quite clear that the velocity field is significantly affected due to permeability and flow separation can be controlled by the permeability of the porous medium in a diverging channel. Figure 5 demonstrates that velocity grows (/decreases) with the suction (/injection) parameter $S > 0$ ($/S < 0$) and corresponding boundary layer turns into thinner (/thicker) one for both nanoparticles cases. This figure also depicts that increment in velocity for Cu-H_2O nanofluid is greater than that of Ag-H_2O nanofluid. This analysis reveals that when permeability parameter K and nanoparticle-volume-fraction-related parameter ϕ_1 are chosen in a way such that they satisfy the condition $K > 2\phi_1$ then boundary layer flow separation is prevented and it allows for a self-similar boundary layer solution with a lower level of suction strength compared with the case $K = 0$ and without nanoparticle, as reported by Holstein [30]. Actually, in diverging channels, existence of boundary layer structure may be controlled by applied suction/injection parameter. Another significant result that emerges from this investigation is that in a diverging channel, boundary layer flow exists even in the presence of mass injection at the walls when $K > 2\phi_1$.

Figures 6–12 explore the impacts of the parameters ϕ, K, S, Ec, n, and Pr on temperature $\theta(\eta)$. Figure 6 shows that temperature and the corresponding thermal boundary layer thickness grow with the volume fraction of nanoparticle ϕ. Also, augmentation of temperature is greater in Ag-H_2O nanofluid when it is compared with Cu-H_2O nanofluid. Temperature profile increases (figure 7) as the permeability parameter increases and this enhancement is more for Ag-

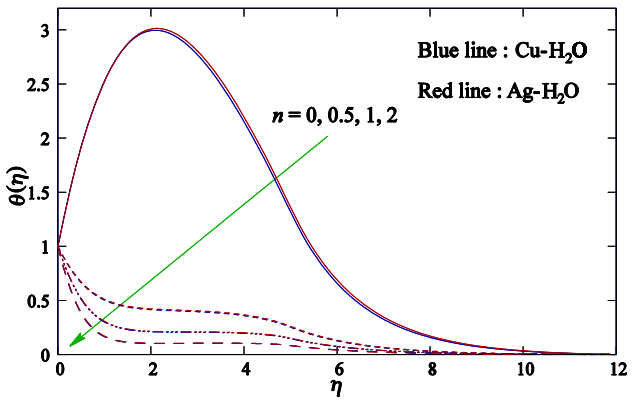

Figure 10. Temperature profile for various values of n with $\phi = 0.1$, $K = 4$, $S = 0.2$, $Ec = 0.03$, and Pr = 6.2.

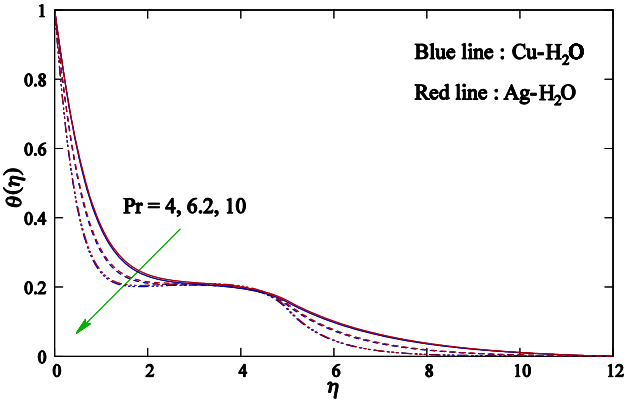

Figure 11. Temperature profile for various values of Pr with $\phi = 0.1$, $K = 4$, $S = 0.2$, $Ec = 0.03$, and $n = 1$.

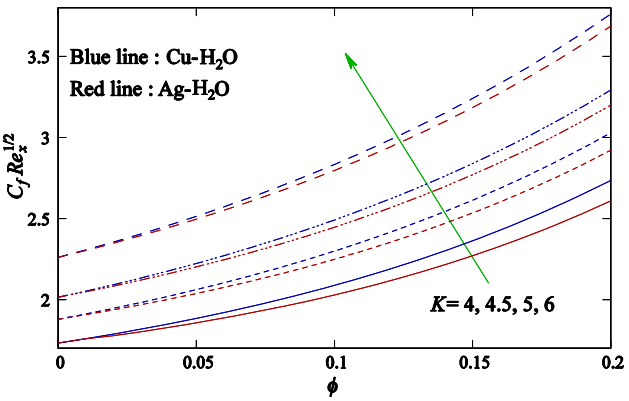

Figure 12. Local skin-friction coefficient for various values of K with ϕ when $S = 0.2$, $Ec = 0.03$, $n = 1$, and Pr = 6.2.

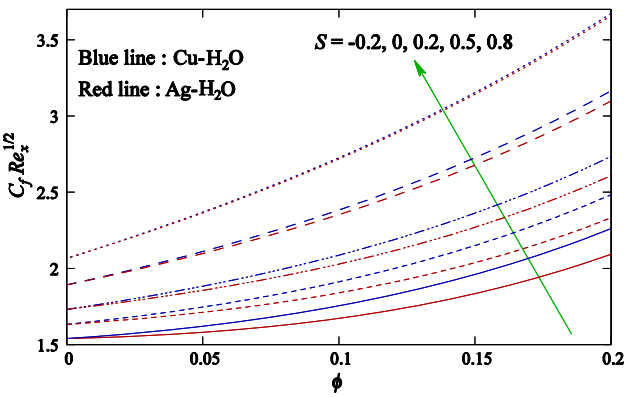

Figure 13. Local skin-friction coefficient for various values of S (suction/injection) with ϕ when $K = 4$, $Ec = 0.03$, $n = 1$, and Pr = 6.2.

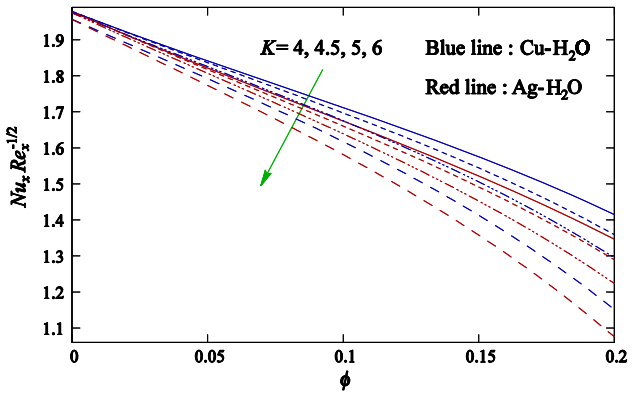

Figure 14. Local Nusselt number for various values of K with ϕ when $S = 0.2$, $Ec = 0.03$, $n = 1$, and $\mathrm{Pr} = 6.2$.

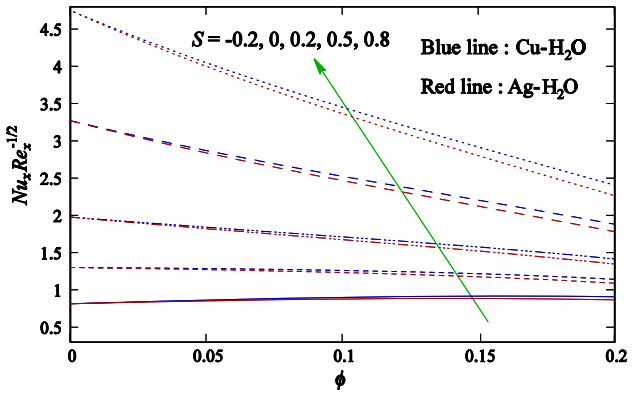

Figure 15. Local Nusselt number for various values of S (suction/injection) with ϕ when $K = 4$, $Ec = 0.03$, $n = 1$, and $\mathrm{Pr} = 6.2$.

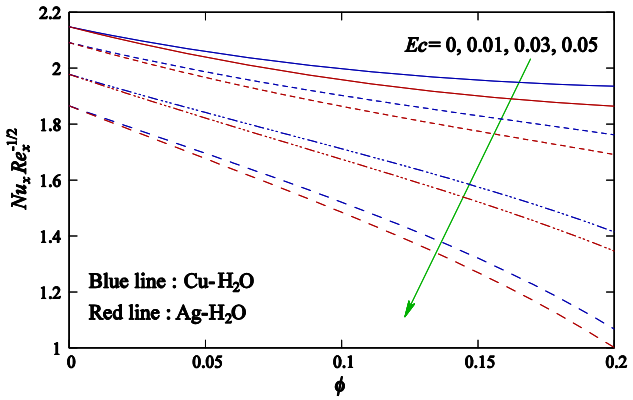

Figure 16. Local Nusselt number for various values of Ec with ϕ when $K = 4$, $S = 0.2$, $n = 1$, and $\mathrm{Pr} = 6.2$.

H_2O nanofluid than Cu-H_2O. From figure 8, it is entirely clear that temperature and corresponding boundary layer thickness are reduced with mass suction/injection parameter S for both nanofluids and the enhancement of temperature in the middle portion is considerably less compared

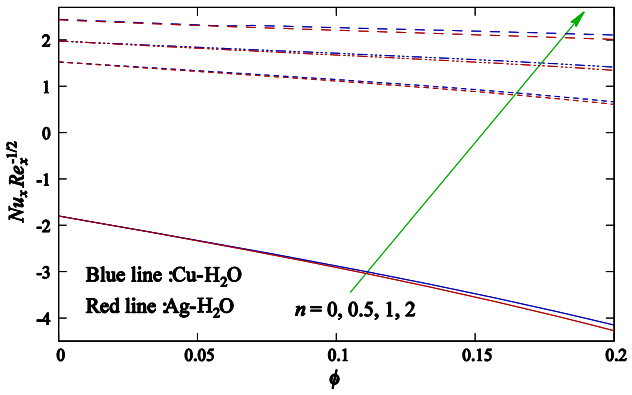

Figure 17. Local Nusselt number for various values of n with ϕ when $K = 4$,$S = 0.2$, $Ec = 0.03$, and $\mathrm{Pr} = 6.2$.

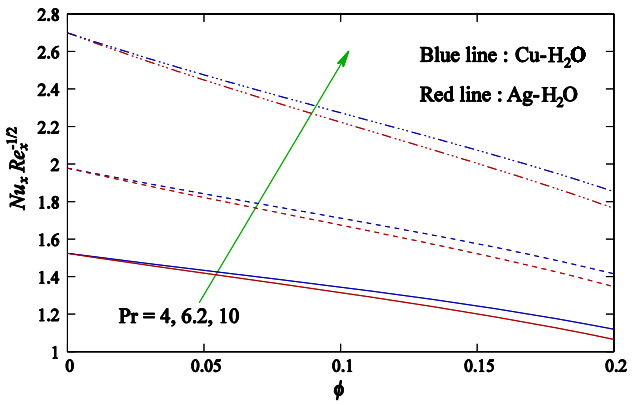

Figure 18. Local Nusselt number for various values of Pr with ϕ, when $K = 4$,$S = 0.2$, $Ec = 0.03$, and $n = 1$.

with near surface and near the free stream. Also, these figures reveal that temperature profile exists for any value of suction/injection parameter S (including $S = 0, -0.2$) unlike the temperature field obtained by Gersten and Korner [31] only when $S \geq 2\sqrt{2}$ in the absence of nanoparticles and Darcy porous medium in the diverging channel [30, 32]. Figure 9 reveals that the temperature profile and the thermal boundary layer enlarge with Ec, and also the impact of Ag-H_2O on temperature profile is more than that of Cu-H_2O. Physically, augmentation in Ec causes increment in kinetic energy; it is well known that average kinetic energy is proportional to temperature field, which increases the temperature. Figure 10 demonstrates that the temperature drops with increase in variable wall-temperature-related power-law exponent n and a temperature overshoot is seen for $n = 0$; also, the corresponding thermal boundary layer becomes smaller with n. Figure 11 displays that both thermal boundary layer and temperature diminish with Prandtl number. Similar to suction/injection parameter, the enhancement in the middle portion of boundary layer is minor when it is compared with that near the surface and near the free stream.

Figures 12 and 13 display the variations of local skin-friction coefficient $C_f \mathrm{Re}_x^{1/2}$ related to surface drag force for the parameters K, S with ϕ. From figure 12, it may be observed that skin friction increases with K and ϕ. From figure 13, it is realized that $C_f \mathrm{Re}_x^{1/2}$ rises gradually with mass suction/injection parameter. Also, from Figures 12 and 13 it is confirmed that for Cu-H_2O nanofluid flow, surface drag force is larger as compared with Ag-H_2O nanofluid and this difference is more for mass injection.

Figures 14–18 present the variations in local Nusselt number ($Nu_x \mathrm{Re}_x^{-1/2}$) with ϕ for various values of K, S, Ec, n, and Pr. The local Nusselt number is related to wall heat transfer rate. Figure 14 reveals that Nusselt number diminishes with ϕ and K. Figure 15 depicts that heat transfer rate increases with mass suction/injection. Figure 16 shows that the Nusselt number decreases with Ec. From Figures 17 and 18, it is found that $Nu_x \mathrm{Re}_x^{-1/2}$ increases with n and Pr. Physically larger Pr values accelerate convective mode of heat transfer, which is proportional to Nusselt number; hence it is augmented. In addition, these figures also reveal that heat transfer rate for Cu-H_2O nanofluid is higher than Ag-H_2O nanofluid [3].

5. Conclusions

The laminar boundary layer flow of water-based nanofluids through a diverging channel in a porous medium with suction/injection has been addressed. The transformed nonlinear ODEs are solved numerically with MATLAB build solver "bvp4c". The main outcomes of the investigation are outlined as follows:

- The boundary layer flow (without separation) in a diverging channel for Newtonian nanofluid in suitable porous medium is possible without any type of condition on suction/injection parameter (i.e., boundary layer separation can be controlled by considering porous medium and nanoparticles).
- The velocity fields for both nanofluids (Cu-H_2O and Ag-H_2O) increase with K and mass suction parameter ($S > 0$), whereas they decrease with ϕ and mass injection parameter ($S < 0$).
- The temperature profile inside boundary layer increases with ϕ, K, Ec, and mass injection $S(<0)$, whereas it reduces with mass suction $S(>0)$, n, and Pr.
- The local skin-friction coefficient, i.e. the surface drag force, increases with ϕ, K, and mass suction $S(>0)$, while the opposite behavior is witnessed for mass injection $S(<0)$.
- The rate of heat transfer increases with mass suction $S(>0)$, n, and Pr, whereas it diminishes with ϕ, K, mass injection $S(<0)$, and Ec.
- The surface drag force and wall heat transfer rate for Cu-H_2O nanofluid are more than those for Ag-H_2O nanofluid.

Acknowledgments

The research of A K Verma is supported by the Council of Scientific and Industrial Research, New Delhi, Ministry of Human Resources Development of India Grant [09/013 (0724)/2017-EMR-I] and the work of A K Gautam is funded by University Grants Commission, New Delhi, Ministry of Human Resources Development, Government of India Grant [1220/(CSIR-UGC NET DEC. 2016)]. The authors are thankful to the anonymous reviewers for their constructive suggestions.

Abbreviations

A_1	Nanoparticle parameter
C_f	Skin-friction coefficient
Ec	Eckert number
f	Dimensionless velocity
k	Variable permeability
k_0	A constant
K	Permeability parameter
L	Characteristic length
n	Power-law exponent
Nu_x	Local Nusselt number
p	Pressure
Pr	Prandtl number
Q	Volume flow rate
q_w	Wall heat flux
Re_x	Local Reynolds number
S	Suction/injection parameter
T	Temperature
T_0	Constant depending upon thermal properties
T_w	Temperature at the surface
T_∞	Ambient temperature
u,v	Velocity components along, respectively, x- and y-axes
U	Free-stream velocity
U_0	Characteristic velocity
v_w	Suction/injection velocity
x, y	Cartesian coordinate measured along the surface and normal to it, respectively

References

[1] Choi S U S 1995 Enhancing thermal conductivity of fluids with nanoparticles. In: Siginer D A and Wang H P (Eds.)

Developments and Applications of Non-Newtonian Flows. New York: ASME, vol. 66, pp. 99–105

[2] Sheikholeslami M, Ganji D D, Ashorynejad H R and Rokni H B 2012 Analytical investigation of Jeffery-Hamel with high magnetic field and nanoparticle by Adomain decomposition method; *Appl. Math. Mech.* **33**(1) 25–36

[3] Usman M, Haq R U, Hamid M and Wang W 2018 Least square study of heat transfer of water-based Cu and Ag nanoparticles along a converging/diverging channel; *J. Mol. Liq.* **249** 856–867

[4] Biswal U and Chakraverty S 2020 Investigation of Jeffery-Hamel flow for nanofluid in the presence of magnetic field by a new approach in the optimal homotopy analysis method; *J. Appl. Comput. Mech.*. https://doi.org/10.22055/jacm.2020.31909.1937

[5] Azimi M and Riazi R 2016 MHD copper-water nanofluid flow and heat transfer through convergent–divergent channel; *J. Mech. Sci. Technol.* **30**(10) 4679–4686

[6] Akinshilo A T, Ilegbusi A, Ali H M and Surajo A J 2020 Heat transfer analysis of nanofluid flow with porous medium through Jeffery-Hamel diverging/converging channel; *J. Appl. Comput. Mech.* **6**(3) 433–444

[7] Alsabery A I, Chamkha A J, Saleh H and Hashim I 2017 Natural convection flow of a nanofluid in an inclined square enclosure partially filled with a porous medium; *Sci. Rep.* **7** 2357

[8] Jeffery J B 1915 The two-dimensional steady motion of a viscous fluid; *Philos. Mag.* **6**(29) 455–465

[9] Hamel G 1916 Spiralförmige Bewegung zäher Flüssigkeiten; *Jahresber. d. Dt. Mathematiker-Vereinigung* **25** 34

[10] Pohlhausen V E 1921 Berechnung der Eigenschwingungen statiisch besiimmter Fachwerke; *Z. Angew. Math. Mech.* **1**(1) 28–42

[11] Millsaps K and Pohlhausen K 1953 Thermal distributions in Jeffery-Hamel flows between non-parallel plane walls; *J. Aeronaut. Sci.* **20** 187

[12] Harrison W J 1919 The pressure in a viscous liquid moving through channel with diverging boundaries; *Proc. Cambridge Philos. Soc.* **19** 307–312

[13] Tollmien W 1921 Gnenzschichtheoric *Handbuch der Experimental Physik*; *Akadeneisahe Verlagsgesellschaft* **4**(1) 241

[14] Noether F 1931 *Handbuch der Physikalischen und Technischen Mechanik*. Leipzig: J. A. Barch, vol. 5, p. 733

[15] Dean W R 1934 Note on the divergent flow of fluid; *Philos. Mag.* **7**(18) 759–777

[16] Bhattacharyya K and Layek G C 2011 MHD boundary layer flow of dilatant fluid in a divergent channel with suction or blowing. *Chin. Phys. Lett.* 28(8): 084705.

[17] Dogonchi A S and Ganji D D 2016 Investigation of MHD nanofluid flow and heat transfer in a stretching/shrinking convergent/divergent channel considering thermal radiation; *J. Mol. Liq.* **224** 592–603

[18] Mohyud-Din S T, Khan U, Ahmed N and Bin-Mohsin B 2017 Heat and mass transfer analysis for MHD flow of nanofluid in convergent/divergent channels with stretchable walls using Buongiorno's model; *Neural Comput. Appl.* **28** 4079–4092

[19] Rana P, Shukla N, Gupta Y and Pop I 2019 Analytical prediction of multiple solutions for MHD Jeffery-Hamel flow and heat transfer utilizing KKL nanofluid model; *Phys. Lett. A* **383**(2–3) 176–185

[20] Kumar K G, Rahimi-Gorji M, Reddy M G, Chamkha A J and Alarifi I M 2020 Enhancement of heat transfer in a convergent/divergent channel by using carbon nanotubes in the presence of a Darcy-Forchheimer medium; *Microsyst. Technol.* **26** 323–332

[21] Jungclaus G 1960 Two-dimensional boundary layers and jets in magneto-fluid dynamics; *Rev. Modern Phys.* **32**(4) 823–827

[22] Layek G C, Kryzhevich S G, Gupta A S and Reza M 2013 Steady magnetohydrodynamic flow in a diverging channel with suction or blowing; *Z. Angew. Math. Mech.* **64** 123–143

[23] Gerdroodbary M B, Takami M R and Ganji D D 2015 Investigation of thermal radiation on traditional Jeffery-Hamel flow to stretchable convergent/divergent channels; *Case Studies Therm. Eng.* **6** 28–39

[24] Adnan Asadullah M, Khan U, Ahmed N and Mohyud-Din S T 2016 Analytical and numerical investigation of thermal radiation effects on flow of viscous incompressible fluid with stretchable convergent/divergent channels; *J. Mol. Liq.* **224** 768–775

[25] Khan U, Adnan Ahmed N and Mohyud-Din S T 2017 Soret and Dufour effects on Jeffery-Hamel flow of second-grade fluid between convergent/divergent channel with stretchable walls; *Results Phys.* **7** 361–372

[26] Nasrin R, Alim M A and Chamkha A J 2013 Effect of heating wall position on forced convection along two-sided open enclosure with porous medium utilizing nanofluid; *Int. J. Energy Technol.* **5**(9) 1–13

[27] Magyari E, Rees D A S and Keller B 2005 Effect of viscous dissipation on the flow in fluid saturated porous media. In: Vafai K (Ed.) *Handbook of Porous Media*, 2nd ed. CRC Press, pp. 373–406

[28] Jafar A B, Shafie S and Ullah I 2020 MHD radiative nanofluid flow induced by a nonlinear stretching sheet in a porous medium. *Heliyon* 6: e04201

[29] Landau L and Lifshitz E M 1959 Fluid Mechanics; Pergamon Press, NY

[30] Holstein H 1943 *Ahnliche laminare Reibungsschichten an durchlässigen Wänden*.ZWB-VM, p. 3050

[31] Gersten K and Körner H 1968 Wärmeübergang unter Berücksichtigung der Reibungswärme bei laminaren Keilströmungen mit veränderlicher Temperatur und Normalgeschwindigkeit entlang der Wand; *Int. J. Heat Mass Transf.* **11**(4) 655–673

[32] Schlichting H and Gersten K 2000 *Boundary layer theory*, 8th; Revised Springer, Berlin